Supplementary information: Revealing the radiative and non-radiative relaxation rates of the fluorescence dye Atto488 in a λ/2 Fabry-Pérot-resonator by spectrally and time resolved measurements†

Alexander Konrad,[a*] Michael Metzger,[a] Andreas M. Kern[a], Marc Brecht[a,b], and Alfred J.Meixner[a‡]

1 Theoretical modeling and analysis

1.1 Free space dipole emitters in the spectral and the time domain

The spectral shape of a vibronic band i in free space and ambient conditions can be approximated by a Gaussian $S_{0_i}(\lambda)$ with amplitude h_{0_i}, spectral position p_i and the full width at half maximum (FWHM) w_i, which is related to the standard deviation c_i. The complete spectrum S_0 for a fluorophore composed of several vibronic bands is then the superposition of all vibronic bands n:

$$S_0(\lambda) = \sum_{i=1}^{n} S_{0_i}(h_{0_i}, p_{0_i}, w_{0_i}, \lambda), \tag{1}$$

with:

$$S_{0_i}(\lambda) = h_{0_i} e^{-(\frac{\lambda - p_i}{2c_i})^2}, \tag{2}$$

$$c_i = \frac{w_i}{2\sqrt{2\ln 2}}, \tag{3}$$

and:

$$\int S_{0_i}(\lambda) d\lambda = h_{0_i} w_i \frac{\sqrt{2\pi}}{2\sqrt{2\ln 2}}. \tag{4}$$

The FWHM is a direct measure for the thermal fluctuations of the energy levels accompanying the transition, wherby the broadening increases most often with increasing energy distance to the 0-0 transition. Further, the integrated intensity of the respective Gaussian i is a measure for the amount of emitted photons for the corresponding spectral transition i with respect to the overall intensity. Thus, the probability of one transition with respect to all other radiative transitions can be given by the ratio:

$$f_{0_i} = \frac{\int S_{0_i}(\lambda) d\lambda}{\int S_0(\lambda) d\lambda}. \tag{5}$$

Regarding the time domain of fluorescent transitons, the excited state X_1 is relaxing to X_0 with a certain rate constant, depending on the relaxation mechanism with its probability. The single radiative transition i occurs with the rate constant k_{r_i} while the non-radiative decay channels are summarized here by the rate constant k_{nr}. The time decay of excited chromophores can be measured by time correlated single photon counting (TCSPC) yielding time dependent decay curves $N(t)$, where $N(t)$ is the number of registered fluorescence photons in the time interval dt. They can be described by the convolution of the pure intensity decay $I_0(t)$ of a chromophore and the instrument response function (IRF) $H(t')$. The most simple decay laws describing $I_0(t)$ are single or multi-exponential functions. The time law for a common chromophore with n vibronic transitions can be derived by stating and solving the differential equation for the time dependent decay of the excited state population X_1:

$$\frac{X_1(t)}{dt} = -(k_{nr} + \sum_{i}^{n} k_{r_i}) X_1(t) = -k_0 X_1(t). \tag{6}$$

By integrating one can find the solution:

$$X_1(t) = e^{-k_{nr}t} \prod_{i}^{n} e^{-k_{r_i}t} = e^{-k_{tot}t}, \tag{7}$$

with k_{tot} as the experimentally accessible total decay constant. Thus, measured decay curves can be described by the convolution of I_0 with the IRF:

$$N(t) = N_0 \int_0^{t'} [e^{-k_{nr}(t-t')} \prod_{i}^{n} e^{-k_{r_i}(t-t')}] H(t') dt', \tag{8}$$

with N_0 as the intensity at $t = 0$. The radiative rate k_{r_i} is directly connected to the spectral intensity of the very same vibronic transition i of the overall spectral intensity. Therefore, the ratio given in equation 5 f_{0_i} can be written also as:

$$f_{0_i} = \frac{k_{r_i}}{\sum k_{r_i}} = \frac{\int S_{0_i}(\lambda) d\lambda}{\int S_0(\lambda) d\lambda}. \tag{9}$$

Together with the quantum yield Ω defined by the ratio of the radiative decay rates and the sum of all decay rates one can write:

$$\Omega = \frac{\sum k_{r_i}}{k_{nr} + \sum k_{r_i}} = \frac{\sum k_{r_i}}{k_{tot}}. \tag{10}$$

1.2 Purcell factor

According to Fermis Golden Rule, the emission properties of a dipole-emitter are depending on the photonic environment. For a two-level system the emission rate of such a transition can be expressed as [1,2]:

$$\Gamma_{spE} = \frac{2\pi}{h^2} |\langle \boldsymbol{\mu} \cdot \boldsymbol{E} \rangle|^2 \rho(\omega). \tag{11}$$

The term in the bra-kets denotes the matrix element of the perturbation between final and initial state, induced by the electric field $\boldsymbol{E}$ and the dipole operator $\boldsymbol{\mu}$. The electric field operator for the spontaneous emission in a Fabry-Pérot cavity can be given analytically [3]. Assuming a cavity with loss-less mirror materials and an isotropic radiating emitter oriented parallel to the y-axis with distance z_0 to the first mirror and an infinitesimally narrow emission

[a] Universität Tübingen, Institut für Physikalische und Theoretische Chemie, Auf der Morgenstelle 18. 72076 Tübingen. Germany.
[b] Process Analysis and Technology (PA&T), Reutlingen Research Institute, Reutlingen University, Alteburgstr. 150, 72762 Reutlingen. Germany.
* alexander.konrad@uni-tuebingen.de
‡ alfred.meixner@uni-tuebingen.de

spectrum, the in-plane electric fields can be calculated for each angle of emission θ and both polarization (s and p) with respect to the mirror surfaces and each emission wavelength given by the k-vector:

$$E^2_{s,||} = \frac{(1-r_{2,s})(1+r_{1,s}-2\sqrt{r_{1,s}}\,\cos(2kz_0\cos\theta)}{(1-\sqrt{r_{1,s}r_{2,s}})^2+4\sqrt{r_{1,s}r_{2,S}}\,\sin^2(kL\cos\theta)}|E_0^2|, \tag{12}$$

$$E^2_{p,||} = \frac{(1-r_{2,p})(1+r_{1,p}-2\sqrt{r_{1,P}}\,\cos(2kz_0\cos\theta)\cos^2\theta}{(1-\sqrt{r_{1,p}r_{2,p}})^2+4\sqrt{r_{1,p}r_{2,p}}\sin^2(kL\cos\theta)}|E_0^2|. \tag{13}$$

Here, $r_{i,p/s}$ denotes the reflectivity of the respective mirror for the polarization p or s, L is the effective cavity length and E_0 the initial field magnitude. To get the wavelength dependent Purcell factor $P(\lambda,L)$ for the dipole emitter, the field has to be integrated over all angles θ for the respective emission wavelengths, averaged for both polarizations. The effective cavity length L can be determined by fitting the expressions for the optical fields to a measured transmission spectrum using reflection coefficients provided by the transfermatrix-method (TMM) and for $\theta = 0$.
Inside a cavity, the radiative rates are specifically altered due to the changed photonic mode density affecting the rate constants and the spectral shape of the fluorescence bands, depending on the resonator length L. For simplicity, the mean Purcell factor is calculated for random dipole orientations ϕ, emission angles θ with respect to the collection efficiency of the objective lens and axial positions of the emitter z_0, which is hosted inside a thin film of several nanometers with a distance of ~ 60 nm to the first mirror. Further the radiative enhancement factor is simplified further as $P(\lambda,L)$.

1.3 Impact on dipole emitters and analysis

The aim is now, to correlate the spectral and temporal information gained by the mirror separation dependent fluorescence spectra and decay curves. The modification of a single vibronic band $S^*_{cav_i}(\lambda,L)$ by the cavity how it appears in an experimental spectrum can be described by the spectral shape S_{0_i} of the radiative transition i weighted by $P(\lambda,L)$ and regarding the detection efficiency of this transition. First, we determine the modified radiative rate constant by the overlapp of the Purcell factor and the spectral band, multiplied by its free space rate k_{r_i}:

$$k^*_{r_i}(L) = k_{r_i}\frac{\int P(\lambda,L)S_{0_i}(\lambda)d\lambda}{\int S_{0_i}(\lambda)d\lambda}. \tag{14}$$

And the modified histogram can be easily given by:

$$N^*(t,L) = N_0^*\int_0^{t'} e^{-k^*_{nr}(L)\cdot(t-t')}\prod_i^n e^{-k^*_{r_i}(L)\cdot(t-t')}H(t')dt', \tag{15}$$

and the total decay rate by:

$$k^*_{tot}(L) = k^*_{nr}(L) + \sum_i^n k^*_{r_i}(L). \tag{16}$$

In analogy to equation 9 we can write:

$$f_i^* = \frac{k^*_{r_i}(L)}{\sum k^*_{r_i}(L)} = \frac{\int S_i^*(\lambda,L)d\lambda}{\int S^*(\lambda,L)d\lambda}. \tag{17}$$

Here, S^* and S_i^* refer to the cavity modified shapes without respect to the detection, because the detection probability should not alter the fluorescence properties of the emitter in the resonator. Since a molecule can also emit into angular distributed off-axis modes, both, the collection efficiency of the objective lense and the asymetry of the spectrally distributed mode spectrum of the cavity affect the shape of the detected spectral band. The fluorescence spectrum can not be regarded as a Gaussian any more, whereby the transition energy p_i and the FWHM w_i of the experimental band $S^*_{cav_i}$ are not altered by the photonic mode density. Therefore, the cavity distorted band $S^*_{cav_i}$ with respect to the complete normalized spectrum can be described by a Gaussian with altered intensity weighted by a normed angular sensitivity function $D_N(\lambda,L)$ and the normed Purcell factor $P_N(\lambda,L)$. The detection function $D(\lambda,L)$ can be calculated by the deviation of the emission angle θ with respect to the on-axis emission and is close to unity for resonant or red shifted wavelengths while it decreases for blue shifted wavelengths. Thus, we first use the scaling factor introduced in equation 17 to account for the altered intensity ratio with respect to the other bands of the complete spectrum:

$$S_i^*(\lambda,L) = f_i^*\frac{S_{0_i}(\lambda)}{\int S_{0_i}(\lambda)d\lambda}P_N(\lambda,L), \tag{18}$$

which leads to:

$$S^*_{cav_i}(\lambda,L) = S_i^*(\lambda,L)D_N(\lambda,L), \tag{19}$$

and finally:

$$S^*_{cav}(\lambda,L) = \sum_i^n S^*_{cav_i}(\lambda,L). \tag{20}$$

In order to correlate now the spectral and temporal information, we connect the intensity ratio for each band with the experimentally accessible total decay rates k_{tot} and $k^*_{tot}(L)$. Therefore, we can express equation 18 in the following way:

$$S_i^*(\lambda,L) = \frac{k^*_{r_i}(L)}{k^*_{tot}(L)-k^*_{nr}(L)}\frac{S_{0_i}(\lambda)}{\int S_{0_i}(\lambda)d\lambda}P_N(\lambda,L), \tag{21}$$

and by using equation 14:

$$S_i^*(\lambda,L) = \frac{k_{r_i}\int P(\lambda,L)S_{0_i}(\lambda)d\lambda}{k^*_{tot}(L)-k^*_{nr}(L)}\frac{S_{0_i}(\lambda)}{(\int S_{0_i}(\lambda)d\lambda)^2}P_N(\lambda,L). \tag{22}$$

Regarding the free space rate $k_{r_i} = f_{0_i}\sum k_{r_i}$ and equation 5 we can further write:

$$S_i^*(\lambda,L) = \frac{\sum k_{r_i}\int P(\lambda,L)S_{0_i}(\lambda)d\lambda}{k^*_{tot}(L)-k^*_{nr}(L)}\frac{S_{0_i}(\lambda)}{\int S_{0_i}(\lambda)d\lambda\int S_0(\lambda)d\lambda}P_N(\lambda,L). \tag{23}$$

The non-radiative rate $k^*_{nr}(L)$ is describable by a model function following the near-field amplitude decay from the molecule to a mirror surface according to L^{-3} [4], an additional scaling factor a and the free space decay rate representing the various non-

radiative decay mechanisms in free space:

$$k^*_{nr}(L) = aL^{-3} + k_{nr}. \tag{24}$$

To final model function can then be expressed with the quantum yield $\Omega = \frac{\sum k_{r_i}}{k_{tot}}$ as:

$$S^*_i(\lambda, L) = \frac{\Omega k_{tot} \int P(\lambda, L) S_{0_i}(\lambda) d\lambda}{k^*_{tot}(L) - (aL^{-3} + (1-\Omega)k_{tot})} \times \frac{S_{0_i}(\lambda) P_N(\lambda, L)}{\int S_{0_i}(\lambda) d\lambda \int S_0(\lambda) d\lambda}. \tag{25}$$

For the equations 25, 19 and 20 the Purcell factor $P(\lambda, L)$ and the detection function $D(\lambda, L)$ are determinable by the model sketched above, the mirror separation L is determinable by measuring the on-axis transmission wavelength, the total decay rates k_{tot} and k^*_{tot} can be determined by evaluating the fluorescence decay curves and the experimental shapes $S^*(\lambda, L)$ and $S_0(\lambda)$ (equation 1) by recording the fluorescence spectra. It can be seen also from equation 25 that all spectra are normed, which leads to a purely dependency on the shaped of the spectra and not on the measured overall intensity.

Now, this set of model functions can be fitted to the experimental data in order to determine the $3n$ parameters for the Gaussians S_{0_i}, the course of the non-radiative decay rate k^*_{nr} and the quantum yield Ω. For minimizing the error and optimizing the fit-paramters (11 parameters for $n = 3$) one needs a large number of datasets at different mirror separations (800 spectra/decay curves for transmission wavelengths between 500 and 700 nm). However, the procedure can be additionally optimized by setting reasonable limits and constraints for the respective parameters. The results for the fitting procedure can be seen in the main article in Figure 2, 3 $(S_{0_i}(\lambda), S^*_{cav_i}(\lambda, L))$ and 5 $(k^*_{r_i}(L), k^*_{nr}(L))$.

2 Experimental Methods

The fluorescence of Atto488 (ATTO-TEC, Siegen, Germany) was examined by a confocal microscope shown in Fig. 1a), after excitation by a 488 nm pulsed laser diode (PicoQuant, LDH-P-C-485) operating with a repetition rate of 40 MHz and a pulse width of ~100 ps (PicoQuant, PDL 828 Sepia II). The laser beam with a power of 20 μW was guided by a beamsplitter (AHF, zt488RDC) to the objective lens (Zeiss, plan-apochromat 63x/1.46 immersion oil), which focuses the excitation beam to a diffraction limited volume within the sample. The subsequent fluorescence was collected by the same objective lens and guided back through a pinhole and a long-pass filter (AHF, F76-490) on the detectors, an APD (Perkin Elmer, SPCM-AQRH) and a spectrograph (Princeton Instruments, Acton SP2500) equipped with a CCD-camera (Princeton Instruments, ProEM). A counting module (PicoQuant, HydraHarp400) recorded the signal of the photodiode in order to perform TCSPC. For free space measurements, a droplet (40 μL) of aqueous solution of Atto488 (with concentration of 1e-7 mol/L diluted in 4% PVA) was spin-coated (5 minutes with 6000 rpm) on a cleaned (with chromosulfuric acid) and washed (with tridistilled water) glass cover slip (Menzel, 22x22 mm) to produce a thin film of several nanometers. For the resonator experiments

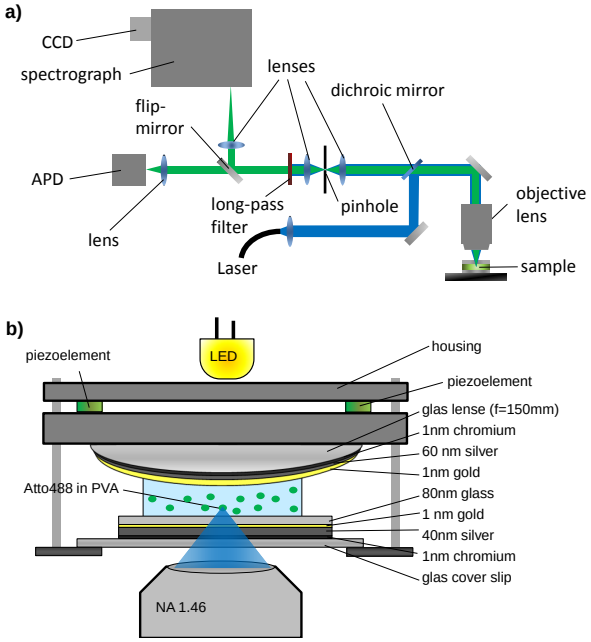

Fig. 1 *Scheme of the experimental setup. a) Scheme of the optical path: The excitation source, a pulsed 488 nm laser diode, is triggered by the Sepia II module which is synchronized with the counter module Hydra Harp 400. The beam is guided by a beamsplitter into the confocal microscope. For excitation and fluorescence collection the same objective (NA=1.46) is used. The fluorescence is deflected through a pinhole and a longpass filter on the detectors, an APD and a spectrograph with equipped thermoelectrically cooled CCD-camera. b) Drawing of the resonator design. The mirrors consist of the following layers: 1) glass cover slide; 2) 1 nm chromium; 3) 40 nm silver; 4) 1 nm gold; 5) 80 nm SiO_2; 6) 1 nm gold; 7) 60 nm silver; 8) 1 nm chromium; 9) glass lens (f=150 mm) hence, the mirror surface can be considered to be parallel within the investigated sample section being less than 100μmin diameter. The cavity length is tuned by the piezoelectric stacks implemented in a mirror mount. The sample is placed about half way between the mirrors on the bottom mirror, which is immersed in the intra-cavity medium (water). The bottom mirror is fixed on a plate which is mounted on a three-axis feed-back controlled scanning stage.*

shown in Fig. 1b), we have used a coated glass cover slip (Menzel, 22x22 mm) and coated glass lens (Thorlabs, LA1433, f=150 mm, R=77.3 mm) as mirrors for the Fabry-Pérot-resonator. The respective layers were deposited on the substrates by electron beam evaporation (Edwards, EB3) monitored by a crystal quartz oscillator with the following sequence: 1 nm chromium, 40 nm silver (60 nm for lens), 1 nm gold and 80 nm glass (for cover slip mirror). The lens was fixed on a kinematic mount including piezoelectric elements (Thorlabs, KC1-T-PZ) in order to alter reproducibly the cavity length. The cavity resonance was checked for every mirror setting by recording white light transmission spectra. Since the radius of the mirror is much larger than the mirror spacing and the diameter of the laser focus the cavity can be described by a plane parallel Fabry-Pérot interferometer with concentric rings fulfilling the idealized resonance conditions $L = m \cdot \lambda/2$ (with $m = 1, 2, 3...$)[5]. The transmission spectra were recorded by illuminating the resonator by a broadband LED from the back side of the resonator. To record fluorescence spectra and

decay curves for different cavity lengths, the fluorophore containing sample was laterally scanned by a feedback controlled piezoelectric scanning stage through the spatially fixed diffraction limited focal confocal volume. The complete setup was controlled by a custom LabView-program allowing us to record a large number of datasets. The data analysis and fitting of the spectra and TCSPC histograms was performed by a custom Matlab program.
For a beam diameter in the resonator of around 500 nm the average number of molecules is roughly 100 (as obtained from spincoating a dye solution with a concentration of $1 \cdot 10^{-7} mol/l$ in 4% PVA) in the detection volume at locations of the sample which yield high fluorescence intensity. With an excitation power of ca. 5 μW entering the resonator we have a photon flux of around $1.25 \cdot 10^{21} ph \cdot s^{-1} \cdot cm^{-2}$. For the excitation wavelength of 488 nm and one molecule with absorption cross section of $3.4 \cdot 10^{-16} cm^{-2}$ this gives an excitation rate between $4.3 \cdot 10^{5} s^{-1}$ (off-resonant) and $8.6 \cdot 10^{6} s^{-1}$ (resonant). Together with the excitation rate and the repetition rate of the laser (40 MHz) we estimate that every pulse excites around 10 molecules.

References

1 E. Fermi, *Rev. Mod. Phys.*, 1932, **4**, 87–132.

2 M. Fox, *Quantum Optics - An Introduction*, Oxford University Press, New York, 2006.

3 G. Bjork, *Ieee Journal of Quantum Electronics*, 1994, **30**, 2314–2318.

4 A. Campion, A. R. Gallo, C. B. Harris, H. J. Robota and P. M. Whitmore, *Chemical Physics Letters*, 1980, **73**, 447–450.

5 S. Bar, A. Chizhik, R. Gutbrod, F. Schleifenbaum, A. Chizhik and A. J. Meixner, *Analytical and Bioanalytical Chemistry*, 2010, **396**, 3–14.